Advanced Functional Materials

ADVANCED FUNCTIONAL MATERIALS
www.afm-journal.de

RESEARCH ARTICLE OPEN ACCESS

Shape-Changing Multiphase Microparticles from Complex Liquid Crystal Emulsions

Marco Turriani[1,2] | Camilla Parmeggiani[2,3] | Daniele Martella[2,3] | Alberto Concellón[4,5]

[1]Dipartimento di Fisica e Astronomia, University of Florence, Sesto Fiorentino, Firenze, Italy | [2]LENS (European Laboratory for Non-Linear Spectroscopy), Sesto Fiorentino, Firenze, Italy | [3]Dipartimento di Chimica "Ugo Schiff", University of Florence, Sesto Fiorentino, Firenze, Italy | [4]Instituto de Nanociencia y Materiales De Aragón (INMA), CSIC-Universidad De Zaragoza, Zaragoza, Spain | [5]Departamento de Química Orgánica, Facultad De Ciencias, Universidad De Zaragoza, Zaragoza, Spain

Correspondence: Daniele Martella (daniele.martella@unifi.it) | Alberto Concellón (aconcellon@unizar.es)

Received: 22 December 2025 | **Revised:** 7 January 2026 | **Accepted:** 15 January 2026

Keywords: adaptive microlenses | complex emulsions | liquid crystal networks | liquid crystals | microactuators | responsive materials | soft robotics

ABSTRACT

Complex multiphase emulsions containing liquid crystals (LCs) offer precise morphological control and dynamic tunability, enabling applications in optics, sensing, and soft matter. Here, we report a simple and scalable bulk-emulsification strategy that circumvents the reliance on microfluidic fabrication to produce liquid crystalline network (LCN) microparticles spanning single, double (Janus), and triple emulsion morphologies within a genuinely colloidal size regime (10–20 μm). By adjusting crosslinking density and interfacial conditions, we program the LC alignment within the droplets, thereby dictating the mode and direction of actuation after photopolymerization. Single emulsions, Janus particles—coupling an active LCN hemisphere to a passive PDMS compartment—and, for the first time, triple LC emulsions—incorporating a third immiscible phase (a fluorinated oil)—are obtained via this straightforward and scalable approach. Across all morphologies, the particles exhibit robust, reversible, large-amplitude deformations under heating, as well as chemoresponsivity through anisotropic swelling in organic solvents. In addition, the Janus particles exhibit gravitational self-orientation, while the triple LC emulsions retain their multiphase architecture and display tunable geometries. As a proof of concept, these responsive behaviors are exploited to realize adaptive microlenses with thermally tunable focal plane and magnification, establishing complex LC emulsions as a scalable platform for multifunctional microactuators.

1 | Introduction

Complex multiphase liquid emulsions (i.e., droplets containing two or more immiscible liquid compartments) are versatile soft matter platforms that have been exploited in a wide variety of fields, from drug delivery to sensing, owing to the precise and dynamic control of their morphology [1]. For example, double emulsions such as water-in-oil-in-water (W/O/W), oil-in-water-in-oil (O/W/O) or oil^1-in-oil^2-in-water (O^1/O^2/W), characterised by an internal protected core, have been studied for encapsulation [2, 3], delivery [4, 5] and controlled release [6–8] of bioactive compounds in food science and medicine. Janus emulsions, consisting of two hemispheres of immiscible liquids, have been exploited as sensors [9–12], active microlenses [13], or responsive inks with tuneable structural color [14] due to their unique ability to undergo morphological reconfiguration in response to external stimuli.

A higher degree of dynamism can be achieved by employing stimuli-responsive materials as the dispersed phase, with liquid crystals (LCs) representing a particularly powerful choice [15, 16]. LCs are soft materials characterised by long-range

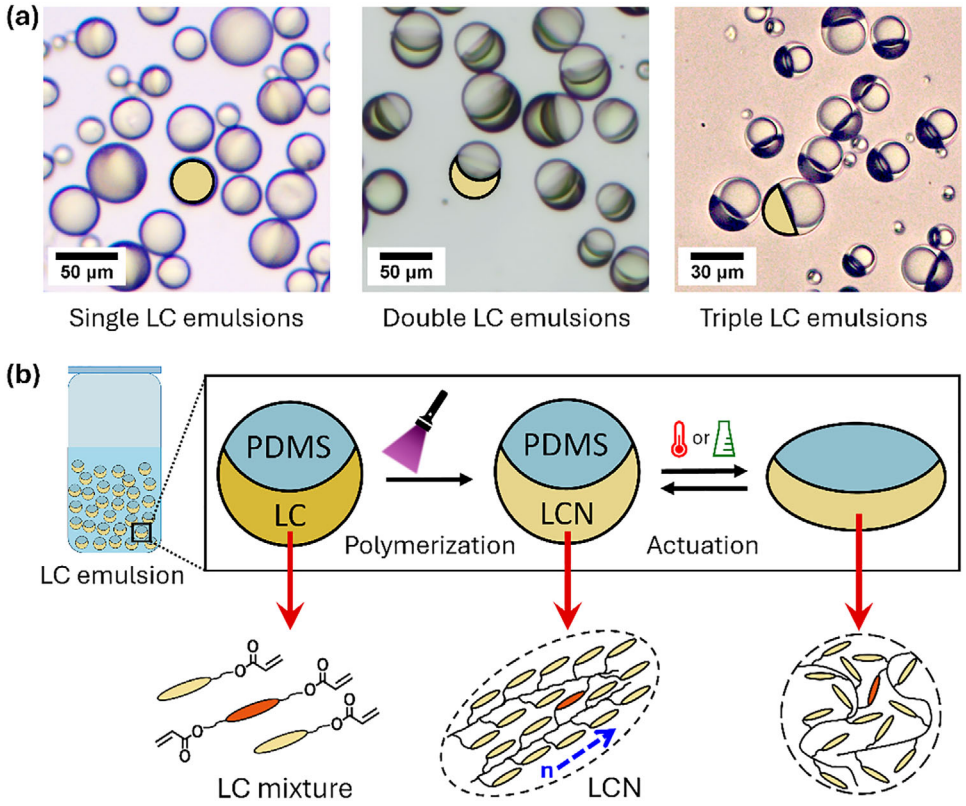

FIGURE 1 | Complex liquid crystal emulsions for the preparation of microparticles with programmed actuation under stimuli. (a) Optical microscopy images of emulsions obtained by bulk emulsification: single, double (Janus), and triple emulsions. The LC phase is highlighted in yellow. (b) Schematic illustration of the preparation of LCN microparticles and their actuation at the microscopic and molecular levels.

molecular order that gives rise to macroscopic anisotropic properties, such as birefringence [17–19]. When dispersed as colloids, LCs self-assemble into different director field configurations depending on the balance between elastic confinement and interfacial anchoring forces at the droplet surface [20–22]. Such complex LC emulsions have been explored as platforms for chemical and biological analyte detection, where small perturbations at the interface induce reorientation of the LC director and a measurable optical response [23, 24].

Few examples have also reported the use of reactive mesogens (i.e., LCs bearing one or more polymerizable moieties) to prepare liquid crystalline networks (LCNs) within emulsion droplets. LCNs are crosslinked materials that deform in a reversible and predictable manner in response to external stimuli [25–27]. For instance, aligned LCNs can contract macroscopically along the nematic director and perform mechanical work when triggered by heat [28, 29], light [30, 31], or chemical inputs [32, 33]. Such actuating LCNs have been widely investigated for applications in soft robotics [34, 35], photonics [36, 37], and biomedicine [38, 39]. In all these systems, precise control over molecular alignment is essential, as it directly determines the direction and magnitude of actuation. Alignment is typically achieved using techniques such as LC cells, photopatterning, or mechanically assisted processing, which rely on specialized instrumentation and therefore limit scalability and the production of large numbers of actuating micro-objects.

In this framework, emulsions of reactive mesogens offer an efficient route to obtain large quantities of LCN microactuators in a straightforward manner, and representative examples from the literature are summarized in Table S1 for comparison. In recent years, several studies have reported on actuating microparticles prepared from single emulsions of reactive LCs [40–45] that can also incorporate functional dopants such as photo-responsive dyes [46] or magnetic nanoparticles [47]. Regarding multiphase complex emulsions, LCN actuators derived from W/O/W systems have been demonstrated to operate as micropumps, expelling the internal liquid phase upon actuation of the LCN shell [48, 49]. Non-spherical Janus particles combining LCNs with hydrogels [50, 51] or silicone oil [52] have also been prepared as microactuators. In the latter case, however, the silicone compartment was subsequently removed, meaning that the final actuating object corresponded to a single-phase LCN particle rather than a true multiphase actuator. To date, examples where the multiple compartments of a complex emulsion are preserved after polymerization and actively participate in actuation remain extremely scarce. Importantly, the reliance on microfluidic fabrication and the resulting large droplet sizes (≈500 µm) limit not only scalability, but also the accessible architectural complexity and functional integration of LC-based microactuators. Moreover, in all these previous examples, reactive mesogen emulsions were produced exclusively by microfluidic techniques. Microfluidics provides exquisite control over droplet size and geometry [53–55], yet it typically yields droplets in the sub-millimeter regime (on the

order of ≈500 μm) and requires specialized instrumentation as well as considerable time to generate large quantities of particles, making scale-up and access to genuinely colloidal dimensions challenging.

Herein, we introduce a simple and scalable bulk emulsification approach to produce single, double, and triple complex emulsions of reactive liquid crystals (Figure 1a), directly addressing the limitations associated with microfluidic fabrication and large droplet sizes in current LC emulsion-based actuators. This strategy enables the rapid preparation of large quantities of LCN microparticles within a colloidal size regime (10–20 μm). Upon photopolymerization, these emulsions yield multiphase LCN microactuators that undergo reversible, directional deformation in response to temperature, and, in some cases, also display chemoresponsivity through anisotropic swelling in organic solvents. By tuning surfactant composition and crosslinking density, we control the internal LC alignment, which in turn dictates the magnitude and the direction of actuation. The resulting particles can exhibit large, fully reversible shape changes, transitioning from spherical to oblate geometries (Figure 1b). Importantly, this strategy enables, for the first time, the fabrication of triple LC emulsions that retain their multi-compartmentalized structure upon polymerization and actively operate as actuators. In addition, the resulting Janus particles exhibit spontaneous gravitational self-orientation, providing a level of collective organization that has not been previously reported. As a proof of concept, we further demonstrate that these multiphase actuators can function as adaptive microlenses, capable of focusing or magnifying projected images under thermal stimulation. This work, therefore, establishes a robust and reproducible route for the scalable production of complex multifunctional LCN microactuators, opening new opportunities in adaptive optics, soft robotics, and responsive microsystems.

2 | Results and Discussion

2.1 | Preparation of Single LC Emulsion-Based Microactuators

LCN microactuators were obtained from single emulsions of reactive mesogens dispersed in an aqueous continuous phase. Different mixtures of polymerizable monomers were formulated by combining a LC monoacrylate (LCm), a LC diacrylate crosslinker (RM257), a radical photoinitiator (BAPO, 5 wt.%), and a radical scavenger (BHT, 1 wt.%) to suppress spontaneous polymerization (Figure 2a). Importantly, the inclusion of the crosslinker RM257 leads, upon UV irradiation, to the formation of a crosslinked polymeric network. To study the effect of crosslinking density on the properties of the final materials, several mixtures were prepared with the amount of crosslinker ranging from 5 wt.% to 20 wt.%. Their mesomorphic behavior was first characterised by polarised-light optical microscopy (POM). In all cases, after melting, the monomer mixtures exhibited the Schlieren textures characteristic of a nematic phase, both during heating and cooling cycles (Figure S1). These observations were consistent with the differential scanning calorimetry (DSC) thermograms, which showed a transition to the nematic phase upon heating (44°C for the 10 wt.% RM257 mixture) and a nematic-to-isotropic transition (57°C for the 10 wt.% RM257 mixture) (Figure S2). Notably, the material did not crystallize at room temperature for several hours. To obtain the emulsions, the protocol illustrated in Figure 2b was followed: LC mixtures were dissolved in dichloromethane (200 mg/mL), added to a 1 wt.% aqueous poly(vinyl alcohol) (PVA) solution, and vortexed at 3000 RPM for 15 s. PVA was employed not only as a stabilizing surfactant to prevent droplet coalescence, but also to promote planar alignment of the LC at the aqueous interface [56].

After dichloromethane evaporation, the droplets exhibited homogeneous spherical morphologies (Figure 2c). Remarkably, in contrast to the bulk LC mixtures, the confined LC droplets did not crystallize for several days, making the emulsions stable over this period. As expected, bulk emulsification produced a broader size distribution compared with microfluidic techniques [57, 58], with droplets displaying an average diameter of 16±6 μm. Despite this dispersity, bulk emulsification is extremely convenient for rapidly obtaining large quantities of droplets owing to its simplicity and scalability.

POM revealed that droplets prepared with 10, 15, or 20 wt.% RM257 displayed diffuse birefringence over the entire droplet surface (Figure 2c; Figures S3 and S4), characteristic of a bipolar configuration. In this arrangement, the director of the nematic LC phase aligns tangentially to the aqueous interface, converging at two point defects (boojums) located at opposite poles. Under crossed polarizers, the birefringence pattern varied with droplet orientation, as expected for bipolar alignment. By contrast, emulsions prepared with 5 wt.% RM257 showed a broader distribution of director configurations, including pre-radial and radial alignments (Figure S5). In this radial configuration, LC molecules are oriented perpendicular to the aqueous interface and converge at a central point defect, giving rise to the characteristic Maltese cross texture under POM. To further clarify the role of the crosslinker, a monomer mixture without RM257 was prepared and emulsified following the same procedure. In this case, the resulting droplets consistently adopted a radial configuration, with a central point defect clearly visible under POM (Figure S6), despite the presence of PVA, which is commonly used to promote planar anchoring. These observations indicate that LC alignment stability in confined droplets is governed by the overall monomer composition rather than by the presence of surfactant alone. Specifically, an intermediate crosslinker fraction (≈10 wt.%–20 wt.%) provides a balance between bulk elastic contributions and interfacial anchoring energies that stabilizes bipolar, actuation-capable director fields, whereas insufficient crosslinker content favors perpendicular anchoring and radial alignment.

To obtain LCN particles, the emulsions were transferred into a Petri dish and photopolymerized under UV at room temperature for 30 min. Indeed, the irradiation caused the photoinitiator decomposition with the consequent free radical polymerization. Successful polymerization was confirmed by ATR-IR spectroscopy, which showed the disappearance of characteristic acrylate bands (1410 cm^{-1}, C═C stretching, and 811 cm^{-1}, ═CH_2 bending) (Figure S6). The polymerised particles retained both the morphology and the LC internal alignment of the precursor droplets. Upon heating, LCN particles containing 10 wt.% RM257 underwent a reversible shape transformation from spherical to oblate. This deformation originates from anisotropic actuation of the LCN: the particles contract along the axis of the nematic

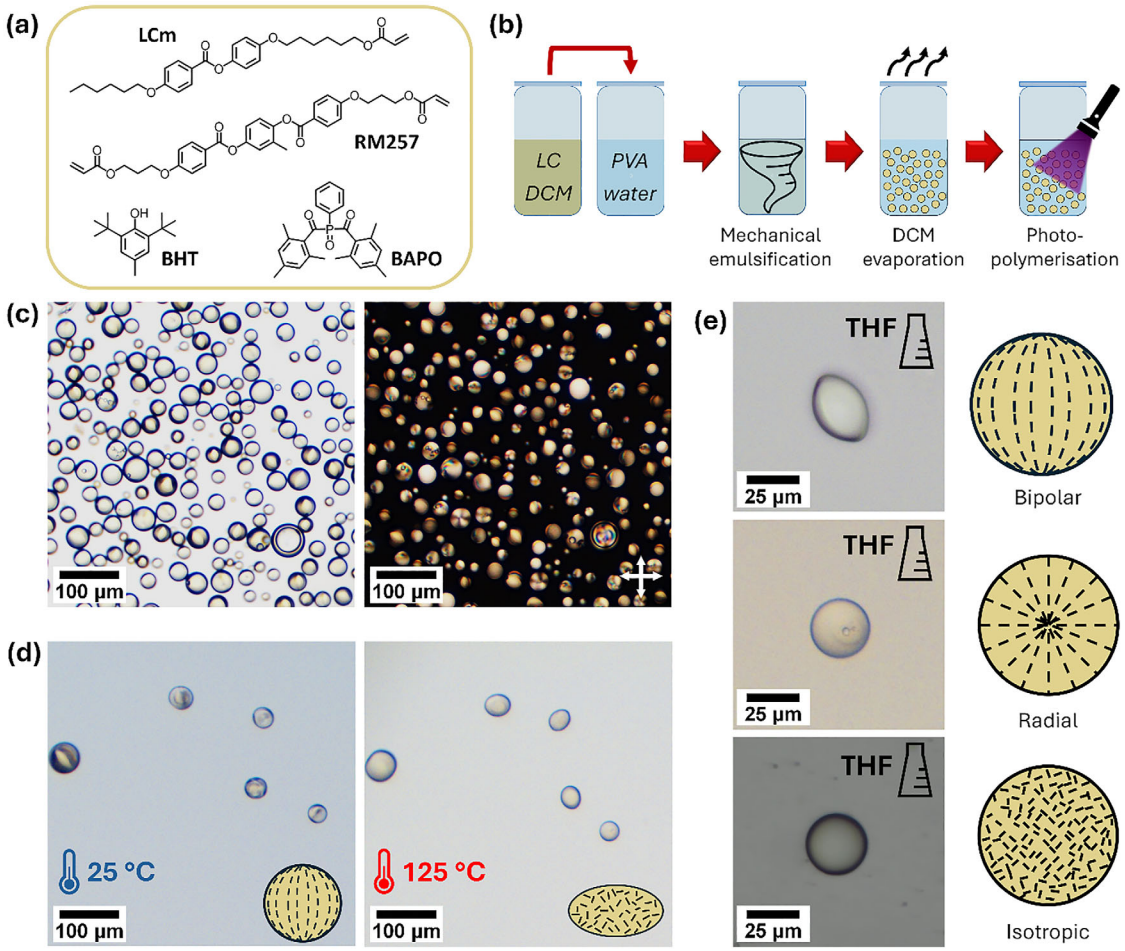

FIGURE 2 | LCN microparticles from a single emulsion. (a) Chemical structures of the polymerizable LC monomer (LCm) and crosslinker (RM257), with RM257 varied from 5 wt.% to 20 wt.%. (b) Schematic representation of the bulk emulsification method used to generate LC droplets and their subsequent photopolymerization into LCN microparticles. (c) Polarized optical microscopy (POM) images of droplets with 10 wt.% RM257 under bright field (left) and crossed polarizers (right), showing bipolar alignment. (d) Thermally induced actuation of LCN microparticles with 10 wt.% RM257, undergoing a reversible spherical-to-oblate deformation upon heating. (e) Swelling of LCN particles with different internal configurations after immersion in THF. From top to bottom: bipolar, radial, and isotropic.

director, resulting in flattening at the poles, and simultaneously expand in the directions perpendicular to the director (Figure 2d; Figure S8). This behavior is analogous to that observed in bulk LC elastomers, where the order-parameter decrease upon heating drives contraction along the director and expansion in the transverse directions. Importantly, this reversible shape change occurs at approximately constant particle volume, as the densities of the nematic and isotropic states are comparable. The aspect ratio, defined as the ratio between major and minor diameters, increased to 1.15±0.09. Upon cooling, the particles recovered their initial shape, demonstrating that the crosslinked network provided sufficient elasticity for fully reversible actuation (Figure S9).

This thermally induced actuation behavior was found to be highly sensitive to crosslinking density. While particles prepared with 10 wt.% RM257 display robust and reproducible actuation, increasing the crosslinker content leads to a progressive suppression of deformation. Particles containing 15 wt.% RM257 still exhibit actuation, but with significantly reduced amplitude compared to the 10 wt.% system, whereas particles prepared with 20 wt.% RM257 show no appreciable deformation under identical conditions (Figure S10). This gradual loss of actuation is attributed to the increasing rigidity of the polymer network, which progressively restricts the ability of the elastomer to undergo macroscopic shape change despite the presence of anisotropic molecular order. Conversely, particles prepared with 5 wt.% RM257 exhibit only weak or sporadic actuation (Figure S11), reflecting insufficient mechanical integrity and the predominance of radial LC configurations, which do not support anisotropic contraction for geometrical reasons.

To demonstrate the tunability of droplet configuration and its direct impact on actuation, we prepared additional samples with identical crosslinker content (10 wt.%) but different LC internal alignments. Radial droplets were obtained by dispersing the already-prepared bipolar emulsion into a 1 wt.% aqueous sodium dodecyl sulfate (SDS) solution prior to polymerization. Under POM, these droplets exhibited a Maltese cross texture centered in the droplet, typical of the radial configuration (Figure S12). In parallel, isotropic particles were produced by photopolymerizing emulsions heated to 65°C, above the nematic-to-isotropic

transition, which resulted in droplets without birefringence upon POM observation. The comparison confirmed that only droplets with bipolar alignment featuring tangential anchoring and boojum defects at opposite poles exhibited reversible anisotropic deformation upon heating, whereas radial or isotropic particles remained spherical and non-actuating.

To further evaluate the structural robustness and responsiveness of the LCN microparticles, we investigated their swelling behavior in tetrahydrofuran (THF). Immersion in THF confirmed that the particles were well crosslinked, as they resisted dissolution in the organic solvent. Interestingly, the swelling profiles strongly depended on the internal LC configuration. Isotropic and radial particles swelled uniformly, preserving their spherical symmetry. In sharp contrast, particles with bipolar alignment exhibited anisotropic swelling, changing their shape from spherical to oblate, in agreement with their behavior under thermal actuation (Figure 2e; Figure S13). These results highlight that anisotropic LC configurations are a prerequisite for directional shape changes under external stimuli and further demonstrate that swelling in organic media provides a form of chemoresponsivity, offering an orthogonal trigger for actuation in LCN microactuators.

2.2 | Preparation of Double LC Emulsion-Based Microactuators

The possibility of obtaining multiphase LCN microparticles from complex LC emulsions was investigated as a strategy to prepare a new class of microactuators with distinct behaviors and functionalities. In this case, double emulsions were produced using the same bulk emulsification procedure described above, but starting from an organic solution containing the LC mixture with 10 wt.% crosslinker and poly(dimethylsiloxane) (PDMS) as a second dispersed phase (Figure 3a). PDMS was selected because it is immiscible with both the LC phase and water, and its fluid nature allows shape-change of the LCN hemisphere without resisting its motion. Moreover, PDMS exhibits a relatively low interfacial tension with nematic LC phases (ca. 5 mN/m), which favors the formation of nearly spherical Janus morphologies [59]. A homogeneous solution was obtained by mixing equal volumes of the LC mixture and PDMS with dichloromethane, which was subsequently emulsified in a 1 wt.% aqueous PVA solution. After solvent evaporation, the droplets separated into two compartments, adopting a Janus morphology. Owing to the slightly higher density of the LC mixture compared to PDMS, the LC hemisphere is preferentially located at the bottom and the PDMS hemisphere at the top. When viewed from above, the droplets appeared perfectly round (Figure 3b); however, side-view observations revealed that the PDMS pole was slightly elongated, giving the droplets a snowman- or dumbbell-shaped Janus morphology (Figure 3c). This slight deviation from a perfectly spherical Janus geometry reflects the finite interfacial tension between the LC and PDMS phases, since an ideal spherical Janus droplet would require a vanishing LC/PDMS interfacial tension (≤ 1 mN/m) [60]. The Janus particles displayed an average diameter of 12±8 μm.

The LC alignment within the Janus droplets was studied by polarized optical microscopy (POM). In the equilibrium configuration, the droplets spontaneously orient under gravity with the LC hemisphere facing downward and the PDMS hemisphere facing upward. In this top-view configuration under crossed polarizers, only the birefringent LC hemisphere is visible, as the PDMS phase is optically isotropic. The LC hemisphere adopts a monopolar configuration, in which the LC director aligns parallel (planar anchoring) to the LC/water interface and perpendicular to the LC/PDMS interface. This internal LC alignment gives rise to the characteristic windmill birefringence pattern, while in bright-field microscopy, a single point defect was localized near the pole of the Janus droplets, corresponding to the junction of the LC directors (Figure 3b). To unambiguously confirm the internal LC alignment, these observations were complemented with side-view POM images (Figure S14). In the side-view geometry, the PDMS hemisphere remains optically isotropic, whereas the LC hemisphere displays low birefringence when the nematic director is nearly parallel to the crossed polarizers and reaches maximum birefringence intensity upon rotating the sample by 45° with respect to the polarizers, in full agreement with the proposed monopolar internal LC organization. Upon UV photopolymerization, the droplets retained both their Janus morphology and their LC alignment, resulting in crosslinked Janus particles with an LCN hemisphere and a fluid PDMS hemisphere. This preservation of morphology and internal configuration is particularly relevant, as it ensures that the final microactuators inherit the anisotropic properties encoded in the LC alignment.

Actuation experiments were performed by heating the Janus particles up to 125°C (Figure 3c; Movie S1). Upon heating, the particles changed shape from nearly spherical to oblate. The LCN hemisphere underwent anisotropic actuation characteristic of LCN: contraction along the nematic director resulted in flattening at the pole (by ~19%), while concomitant expansion perpendicular to the director led to lateral broadening at the equator (by ~11%) (Figure S8). The PDMS hemisphere firmly adhered to the LCN phase and followed this deformation without detaching or disassembling. Upon cooling, the particles returned to their original spheroidal shape, demonstrating fully reversible actuation (Figure S9). Notably, the incorporation of the low-density PDMS phase induced spontaneous gravitational orientation of the Janus droplets, thereby enabling collective actuation along the same axis for all particles. This self-orientation represents a key advantage, opening the door to new applications that require controlled and synchronized microactuation.

Unlike spherical single droplets, Janus droplets are not constrained by perfect spherical symmetry, which makes it possible to exploit radial LC alignment for actuation. Attempts to induce a radial configuration by adding SDS to the aqueous continuous phase led to morphology changes and droplet destabilization. By contrast, when a few drops of ethanol were added to the continuous phase, the LC alignment switched from monopolar to radial. Under crossed polarizers in top-view, the droplets displayed the Maltese cross texture typical of radial configuration, in which LC molecules anchor perpendicular to the aqueous interface (Figure 3d). This radial configuration was further confirmed by side-view POM observations, which also revealed Maltese cross birefringence patterns consistent with a radially oriented director field throughout the LC hemisphere

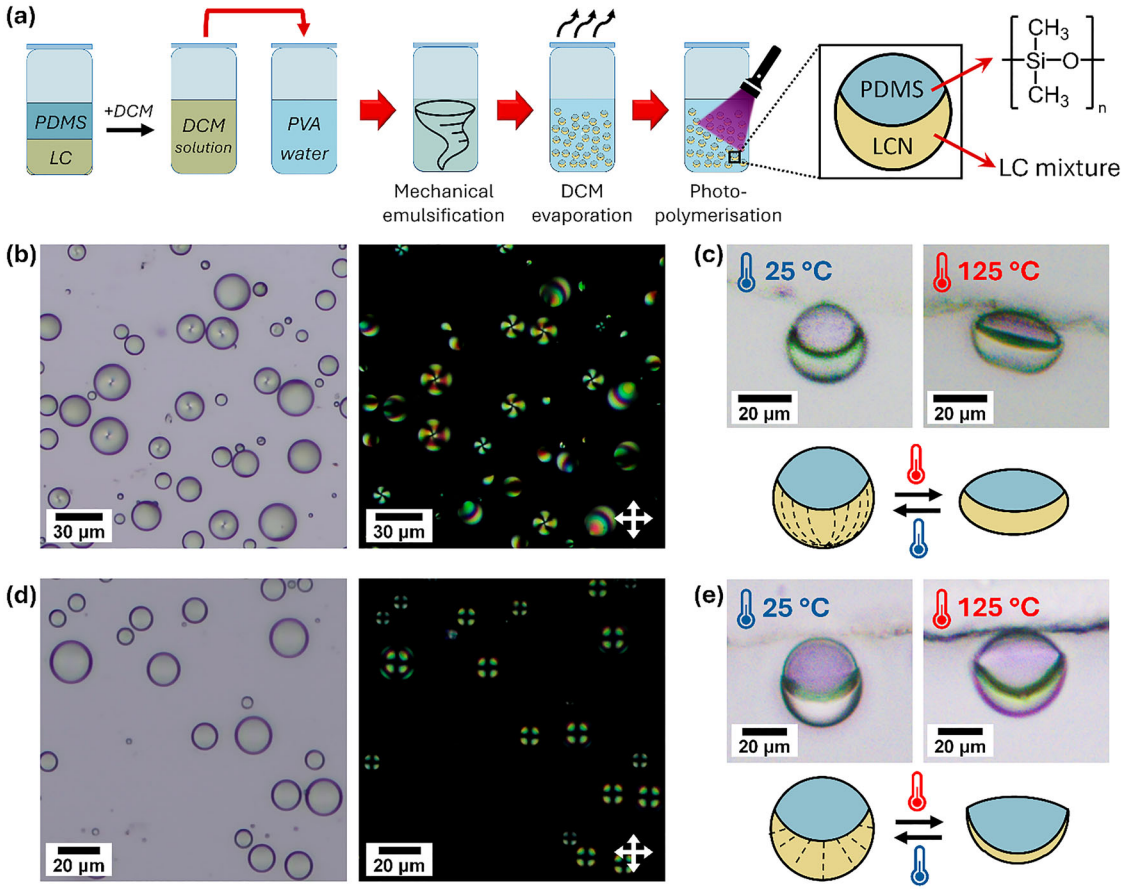

FIGURE 3 | LCN microactuator from double emulsions. (a) Schematic illustration of the bulk emulsification method and components used to generate biphasic LC/PDMS emulsion droplets. (b) Polarized optical microscopy (POM) images of Janus droplets under bright field (left) and crossed polarizers (right), showing the LCN hemisphere in a monopolar configuration. (c) Thermally induced actuation of LCN Janus particles with monopolar LC alignment, undergoing reversible spherical-to-oblate deformation. (d) Polarized optical microscopy (POM) images of Janus droplets under bright field (left) and crossed polarizers (right), showing the LCN hemisphere with radial alignment. (e) Thermally induced actuation of radially aligned Janus particles, leading to a vase-like deformation with PDMS encapsulated within the LCN hemisphere.

(Figure S15). After photopolymerization, these radially aligned Janus particles exhibited a distinctive thermo-responsive behavior: the LCN hemisphere deformed into a vase-like shape, becoming slightly larger (~15%) with thinner walls and a concavity at the center, while the PDMS phase filled this cavity and became more encapsulated within the LCN (Figure 3e). When cooled back to room temperature, the radial particles recovered their original spheroidal morphology, confirming the reversibility of the actuation (Figure S9). The vase-like deformation observed at high temperature can be rationalized by the simultaneous action of two driving forces: (i) anisotropic actuation of the radially aligned LCN hemisphere, in which contraction along the local nematic director (oriented perpendicular to the aqueous interface) is accompanied by expansion in the tangential directions, leading to thinning of the LCN hemisphere (Figure S8), and (ii) a reduction in the relative interfacial tension between PDMS and LCN upon heating. The latter effect was corroborated by independent experiments on unpolymerized Janus droplets, where the PDMS phase became progressively more encapsulated within the LC phase at elevated temperatures, evidencing an increase in mutual affinity between the two liquids (Figure S16).

2.3 | Preparation of Triple LC Emulsion-Based Multiphase Microactuators

More complex droplet morphologies can introduce new characteristics and functionalities into multiphase particles, and the incorporation of a third dispersed phase within droplets provides a straightforward strategy to achieve this goal [61]. Triple emulsions were obtained by mixing the LC phase with PDMS and 2-(trifluoromethyl)-3-ethoxydodecafluorohexane (HFE-7500), a fluorinated oil (FC) immiscible with both the LC and PDMS phases (Figure 4a). A homogeneous solution was first prepared by dissolving the three phases in dichloromethane (200 mg/mL), which was then emulsified in a 1 wt.% aqueous PVA solution. After solvent evaporation, droplets with spherical morphology and three phase-separated compartments were obtained: the LC and PDMS arranged in a Janus-like configuration, while the FC phase was fully encapsulated between them (Figure 4b). This arrangement minimizes the overall interfacial energy by avoiding direct contact between the FC phase and water, which is energetically unfavorable due to the high FC/water interfacial tension (≈40 mN/m) [62]. Under these conditions, PVA stabilizes both the LC and PDMS phases at the aqueous interface in a

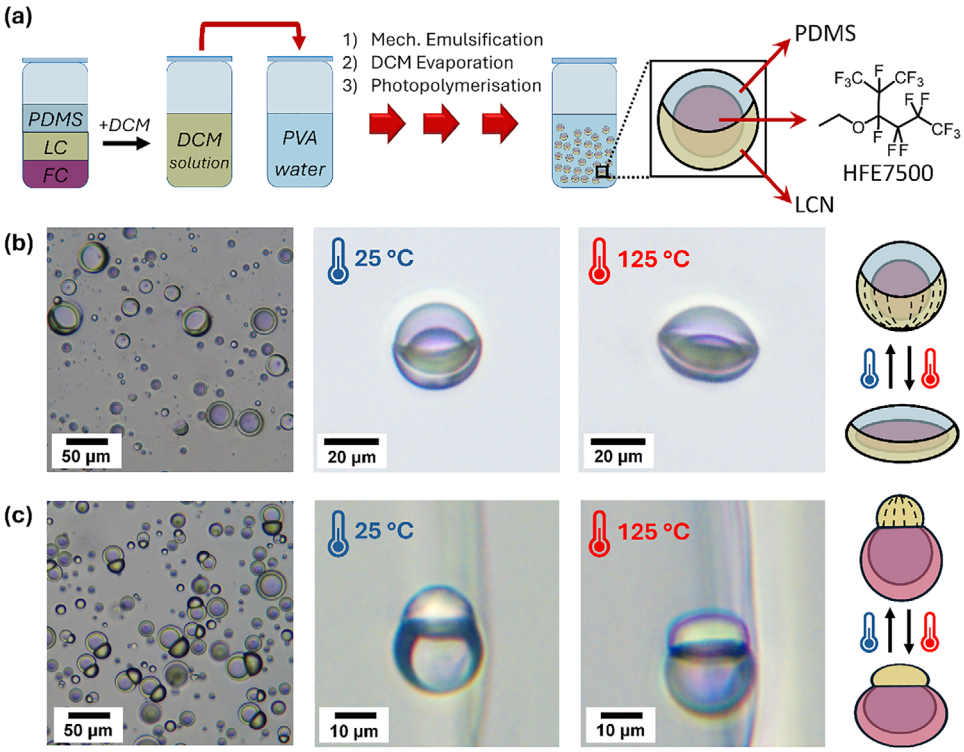

FIGURE 4 | LCN microparticles from triple emulsions. (a) Schematic illustration of the bulk emulsification method and components used to generate triphasic LC/PDMS/HFE-7500 emulsion droplets. (b) Optical microscopy images of spherical triphasic droplets and their thermally induced reversible actuation. (c) Optical microscopy images of triphasic with snowman-like morphology and their corresponding thermal actuation.

comparable manner, leading to a morphology closely resembling that of the corresponding double emulsions, but with the FC phase encapsulated. This configuration is favored by the relatively low interfacial tension between FC and PDMS (≈3 mN/m) and its comparatively low interfacial tension with the LC phase (≈7–8 mN/m) [60].

An alternative morphology could be obtained by reducing the FC/water interfacial tension, for instance by adding specific fluorosurfactants. When 0.1 wt.% Zonyl FS-300, a poly(tetrafluoroethylene)-*block*-poly(ethylene glycol) fluorosurfactant, was introduced into the aqueous continuous phase, the FC phase became preferentially exposed at the droplet surface. As a consequence, the PDMS phase became increasingly encapsulated within the FC compartment owing to its particularly low interfacial tension with FC. This redistribution of the phases drives a transition toward a snowman-like geometry, in which the LC and FC phases form distinct lobes (Figure 4c). The more pronounced snowman-like shape reflects the higher interfacial tension between the LC and FC phases relative to the LC/PDMS interface, highlighting the tunability of these triple emulsions through selective modulation of the interfacial balance by appropriate surfactants.

For both morphologies, the internal LC alignment was investigated by POM using both top- and side-view configurations (Figures S17 and S18). In all cases, the LC hemisphere adopted a monopolar configuration, in which the nematic LC director aligns parallel (planar anchoring) to the aqueous interface and perpendicular to the interface with the PDMS and/or FC phases. This arrangement leads to a single point defect localized near the pole of the LC domain. Under crossed polarizers in the top-view geometry, the droplets displayed characteristic windmill-like birefringence textures. In the side-view configuration, the LC hemisphere exhibited low birefringence when the director was nearly parallel to the polarizer axes, with a maximum birefringence intensity observed upon rotating the sample by 45°, fully consistent with the proposed monopolar internal LC organization. After UV photopolymerization, the droplets retained both their morphology and their LC alignment, yielding stable multiphase microparticles.

The actuating behavior of these particles was tested under heating. Upon increasing the temperature up to 125 °C, the Janus-like triple emulsions deformed from spherical to oblate. This deformation is governed by the anisotropic actuation of the LCN phase: contraction along the nematic director results in flattening at the poles, while the concomitant expansion perpendicular to the director leads to lateral broadening at the equator (Figure S8). Accordingly, the LCN hemisphere expanded laterally (~16%) and flattened at the poles (~15%), while the internal FC compartment followed the deformation and changed accordingly (Figure 4b; Movie S2). In the case of the snowman-like morphology, the LCN hemisphere became significantly flatter at the pole and larger (~31% increase), whereas the passive compartment (PDMS + FC) displayed only minimal deformation (~1%), consistent with its limited contact surface with the active LCN part (Figure 4c). Upon cooling back to room temperature, the triple-emulsion morphologies fully recovered their original shapes, confirming the reversibility of the actuation (Figure S9). These results confirm that the anisotropic contraction of the LC network governs the overall shape change, while the passive compartments

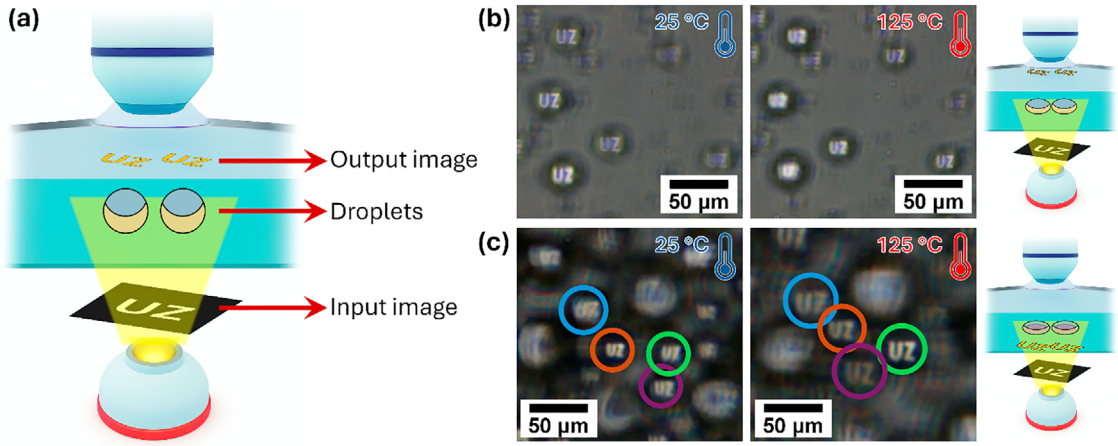

FIGURE 5 | LCN micro-particles as tuneable optical devices. (a) Schematic illustration of the custom optical setup used to evaluate droplet lensing behavior. A well-defined image plane above the sample plane was obtained by focusing the mask projection through the droplets. (b) Images projected by biphasic monopolar particles at room temperature (left) and during thermal actuation at 125°C (center), together with a schematic representation of the optical effect (right). (c) Images projected by triphasic particles at room temperature (left) and during thermal actuation at 125°C (center), together with a schematic representation of the optical effect (right).

adapt their geometry according to their interface with the LCN phase.

2.4 | LCN Microactuators as Adaptive Microlenses

Micro-optical components are fundamental for the development of miniaturized technologies in fields such as imaging, biosensing, and photonics [63, 64]. In particular, micrometric refractive elements that can dynamically change their curvature or morphology offer unique opportunities as tuneable optical devices [13, 65]. Complex LC emulsions are well suited for this role, since their anisotropy, curved interfaces, and responsiveness to external stimuli make them promising building blocks for adaptive micro-optics. We therefore explored the potential of our LCN microactuators as stimuli-responsive optical elements, demonstrating a proof-of-concept for adaptive imaging.

To assess their optical performance, we designed a simple custom setup in which a 3D-printed mask was placed over the light source of a conventional bright-field optical microscope (Figure 5a). When observed under the microscope, each droplet acted as a microlens capable of focusing the projected pattern. A well-defined image plane was identified above the sample, where the mask projection appeared in sharp focus through the droplets. This straightforward arrangement allowed us to directly visualize how droplet morphology modulates light focusing at the microscale.

We first investigated double-phase Janus particles with planar LC alignment, chosen for their pronounced actuation and self-orienting behavior, which ensures spatial control of their optical response. Upon heating, the LCN hemisphere contracted along the nematic director, modifying the radius of curvature of the droplet. As a consequence, the focal plane of the projected image shifted vertically (Figure 5b; Movie S3). Cooling reversed the deformation, restoring both the original droplet shape and the focal plane, thereby confirming the fully reversible nature of this actuation. In this configuration, the droplets function as adaptive microlenses with a tunable focal distance that can be dynamically modulated by temperature.

We then extended the experiment to triple-emulsion particles to evaluate the effect of higher structural complexity. As with Janus droplets, each triple droplet acted as a microlens, but in this case, a second image plane appeared below the droplet plane due to partial light reflection. This effect was more pronounced than in double emulsions, likely arising from the presence of multiple internal interfaces. Upon heating, the projected images were magnified by a magnification factor of 1.5±0.2, and the original dimensions were recovered upon cooling (Figure 5c; Movie S4). This proof-of-concept demonstrates that complex LCN-based droplets can serve as temperature-responsive microlenses with reversible focusing and magnification, establishing multiphase LCN microparticles as a scalable platform for reconfigurable micro-optical systems with potential impact in next-generation imaging and biosensing technologies.

3 | Conclusion

In conclusion, we have developed a simple and scalable bulk-emulsification strategy to fabricate LCN microactuators from single, double, and triple LC emulsions, overcoming the reliance on microfluidic instrumentation and enabling access to genuinely colloidal, architecturally complex actuating particles (10–20 µm), in contrast to previous approaches that rely almost exclusively on microfluidics and typically yield sub-millimeter LC particles (ca. 500 µm). By tuning crosslinking density and interfacial conditions, we established a direct correlation between LC alignment and actuation performance. In single emulsions, a crosslinker content of 10 wt.% provides an optimal balance between alignment stabilization and network elasticity, enabling fully reversible anisotropic deformation, whereas higher crosslinking densities or radial alignment suppress actuation. Extending this concept to multiphase droplets, Janus particles combine an active LCN hemisphere with a passive PDMS phase that follows its motion and, uniquely, enables spontaneous gravitational

self-orientation for collective actuation. Furthermore, reconfiguring the LC alignment from monopolar to radial prior to curing yields distinct thermoresponsive deformation modes. Introducing a third immiscible phase (a fluorinated oil such as HFE-7500) yields triple LC emulsions with tunable morphologies (Janus-like and snowman-like) controlled by fluorosurfactants. To the best of our knowledge, this constitutes the first demonstration of triple LC emulsions that retain all compartments after polymerization and operate as reversible actuators, exhibiting robust, fully reversible, large-amplitude shape changes (spherical-to-oblate) under heating.

As a proof of concept, we further demonstrate that these multiphase LCN particles can function as adaptive microlenses, enabling fully reversible tuning of focal plane or magnification and underscoring their potential in reconfigurable micro-optics. Together, these results establish complex LC emulsions as a versatile and scalable platform for multifunctional microactuators, expanding their application scope beyond previously proposed micropumping or robotic concepts. Future work will focus on expanding responsiveness beyond temperature to light, pH, and chemical cues, and on integrating these actuators into arrays and device architectures, opening pathways toward advanced applications in adaptive optics, soft robotics, and biosensing.

4 | Experimental Section

4.1 | Materials

The LC monomer 4-((6-(Acryloyloxy)hexyl)oxy)phenyl 4-(hexyloxy)benzoate (namely LCm) and the LC crosslinker 2-methyl-1,4-phenylene bis(4-(3-(acryloyloxy)propoxy)benzoate) (RM257) were purchased from Synthon Chemicals ($\rho \approx$ 1.0 g/mL at 25°C). The radical photoinitiator phenylbis(2,4,6-trimethylbenzoyl) phosphine oxide (BAPO), 2,6-di-tert-butyl-4-methylphenol (BHT), poly(vinyl alcohol) (PVA), sodium dodecyl sulfate (SDS), and dichloromethane were purchased from Sigma–Aldrich. Poly(dimethylsiloxane) (PDMS, 350 cSt; ρ = 0.965 g/mL at 25°C), and dichloromethane was purchased from Fisher Scientific, 2-(Trifluoromethyl)-3-ethoxydodecafluorohexane (HFE7500; ρ = 1.60 g/mL at 25°C) was purchased from Flurochem. All the chemicals were used as received without further purification.

4.2 | Microactuator Preparation

First, a monomer solution has been obtained by mixing LCm (41.5 mg, 0.089 mmol), RM257 (5.0 mg, 0.0085 mmol), BAPO (2.5 mg, 0.006 mmol), and BHT (1.0 mg, 0.0045 mmol) with 0.5 mL of dichloromethane. The solvent was then evaporated, and the mixture was dried under vacuum.

To obtain single emulsions, 75 µL of the monomer solution (20 mg of the monomer mixture in 0.1 mL of dichloromethane) was poured into an ambered vial with 1 mL of PVA solution in water (1% weight). The biphasic mixture was emulsified through a CLASSIC vortex mixer from Velp at 3000 rpm for 15 s. Dichloromethane has been left evaporating at RT overnight over an orbital agitator. The droplets were then transferred to a petri dish and subjected to photopolymerization for 30 min using a Philips PL-S-9 W UV Hg lamp with a maximum emission at 365 nm. Droplets with different compositions were prepared following the same procedure and using the different monomer mixtures reported in Table S2.

To obtain double emulsions, the initial monomer solution was composed of 10 mg of the LC mixture plus 10 mg of PDMS dissolved in 0.1 mL of dichloromethane. Then, the same procedure described above was followed to obtain the emulsion and the relative polymerized micro-particles.

To obtain triple emulsions, the initial monomer solution was composed of 10 mg of the LC mixture, plus 10 mg of PDMS and 10 µL of HFE7500 dissolved in 0.15 mL of dichloromethane. Then the same procedure described above was followed to obtain the emulsion and the relative polymerized micro-particles.

4.3 | Microactuator Characterization

The LC mixtures, the emulsions, and the LCN particles were characterized with a polarized-light optical microscopy (POM) on an Olympus BH-2 polarizing microscope equipped with a Linkam THMS600 hot stage. Side-view images of the droplets were taken using a custom-built horizontal AmScope PZ200 polarizing microscope. For these experiments, emulsion droplets were deposited into a demountable quartz cuvette (path length: 100 µm) from Hellma. The thermal analysis was conducted through a differential scanning calorimeter (DSC, Thermal analysis TA Q2000). The Attenuated total reflectance infrared spectra (ATR-IR) were recorded using a spectrophotometer Shimadzu IRAffinity-1S. Thermal actuations were evaluated by optical microscopy and imaged by immersing the droplets in glycerol and then, heating the dispersion up to 125°C.

Acknowledgements

A.C. thanks financial support from the projects PID2023-146811NA-I00 and RYC2021-031154-I, funded by MICIU/AEI/10.13039/501100011033 and "ERDF: A way of making Europe"; from the Fundación Ramón Areces through the XXII Concurso Nacional de Ciencias de la Vida y de la Materia (project CIVP22A7601); and from the Gobierno de Aragón–FSE (research group E47_23R). C.P. acknowledges financial support from the project "ALICE" (proposal code 20224EBZ3Y – CUP J53D23008450006) granted by the European Union - NextGenerationEU under the National Recovery and Resilience Plan (PNRR) - Mission 4 Education and research - Component 2 From research to business - Investment 1.1 Notice Prin 2022 - DD N. 104 del 02/02/2022, and the financial support provided by the MUR – Dipartimenti di Eccellenza 2023-2027 (DICUS 2.0) to the Department of Chemistry "Ugo Schiff" of the University of Florence. The authors gratefully acknowledge the use of SAI (UNIZAR) and CEQMA (UNIZAR-CSIC) Services. INMA acknowledges financial support from the "Severo Ochoa" Programme for Centres of Excellence in R&D (CEX2023-001286-S), funded by MICIU/AEI/10.13039/501100011033.

Conflicts of Interest

The authors declare no conflicts of interest.

Data Availability Statement

The data that support the findings of this study are available in the supplementary material of this article.

References

1. A. Aserin, ed., *Multiple Emulsions: Technology and Applications* (Wiley-Interscience, 2008).

2. T. Cetinkaya, F. Altay, and Z. Ceylan, "A New Application With Characterized Oil-In-Water-In-Oil Double Emulsions: Gelatin-Xanthan Gum Complexes For The Edible Oil Industry," *LWT* 138 (2021): 110773.

3. C. Kabakci, G. Sumnu, S. Sahin, and M. H. Oztop, "Encapsulation of Magnesium With Lentil Flour by Using Double Emulsion to Produce Magnesium Enriched Cakes," *Food and Bioprocess Technology* 14 (2021): 1773–1790, https://doi.org/10.1007/s11947-021-02672-5.

4. C. Cimino, A. Bonaccorso, B. Tomasello, et al., "W/O/W Microemulsions for Nasal Delivery of Hydrophilic Compounds: A Preliminary Study," *Journal of Pharmaceutical Sciences* 113 (2024): 1636–1644, https://doi.org/10.1016/j.xphs.2024.01.013.

5. M. Li, B. Xie, M. Wang, J. Ju, Y. Zhang, and Y. Ma, "Construction and application of a W1/O/W2 emulsion based co-delivery system for Polygonatum saponins and polysaccharides," *LWT* 231 (2025): 118320, https://doi.org/10.1016/j.lwt.2025.118320.

6. S. M. Ferreira, L. Tavares, and L. Santos, "Enhanced Microencapsulation of Quercetin-Rich Onion (Allium cepa) Peel Extract in Ethyl Cellulose Using a W/O/W Double Emulsion: Optimised Production, Characterisation, and Controlled Release," *Journal of Polymers and the Environment* 33 (2025): 2567–2586, https://doi.org/10.1007/s10924-025-03552-1.

7. J. Liu, M. Kharat, Y. Tan, H. Zhou, J. L. Muriel Mundo, and D. J. McClements, "Impact of Fat Crystallization On The Resistance Of W/O/W Emulsions To Osmotic Stress: Potential For Temperature-Triggered Release," *Food Research International* 134 (2020): 109273, https://doi.org/10.1016/j.foodres.2020.109273.

8. S. Zhang, R. Yan, S. Zhang, and Y. Lu, "W/O/W Multiple Emulsified Microcapsules Based on Biopolymer Soybean Isolate Proteins: Improving Tannic Acid's Biocompatibility and Sustained-Release Performance," *Molecules (Basel, Switzerland)* 30 (2025): 2373, https://doi.org/10.3390/molecules30112373.

9. D. Fong and T. M. Swager, "Trace Detection of Hydrogen Peroxide via Dynamic Double Emulsions," *Journal of the American Chemical Society* 143 (2021): 4397–4404, https://doi.org/10.1021/jacs.1c00683.

10. L. Zeininger, S. Nagelberg, K. S. Harvey, et al., "Rapid Detection of Salmonella enterica via Directional Emission From Carbohydrate-Functionalized Dynamic Double Emulsions," *ACS Central Science* 5 (2019): 789–795, https://doi.org/10.1021/acscentsci.9b00059.

11. J. Li, A. Concellón, K. Yoshinaga, Z. Nelson, Q. He, and T. M. Swager, "Janus Emulsion Biosensors for Anti-SARS-CoV-2 Spike Antibody," *ACS Central Science* 7 (2021): 1166–1175, https://doi.org/10.1021/acscentsci.1c00173.

12. L. D. Zarzar, J. A. Kalow, X. He, J. J. Walish, and T. M. Swager, "Optical Visualization And Quantification Of Enzyme Activity Using Dynamic Droplet Lenses," *Proceedings of the National Academy of Sciences* 114 (2017): 3821–3825, https://doi.org/10.1073/pnas.1618807114.

13. S. Nagelberg, L. D. Zarzar, N. Nicolas, et al., "Reconfigurable and Responsive Droplet-Based Compound Micro-Lenses," *Nature Communications* 8 (2017): 14673, https://doi.org/10.1038/ncomms14673.

14. A. E. Goodling, S. Nagelberg, B. Kaehr, et al., "Colouration by Total Internal Reflection And Interference At Microscale Concave Interfaces," *Nature* 566 (2019): 523–527, https://doi.org/10.1038/s41586-019-0946-4.

15. A. Concellón, "Liquid Crystal Emulsions: A Versatile Platform For Photonics, Sensing, And Active Matter," *Angewandte Chemie International Edition* 62 (2023): 202308857.

16. A. Terrel, S. Del Moral, A. Martínez-Bueno, and A. Concellón, "Dynamically Reconfigurable Complex Liquid Crystal Emulsions," *Liquid Crystals* 51 (2024): 2321–2338, https://doi.org/10.1080/02678292.2024.2325587.

17. P. J. Collings and J. W. Goodby, *Introduction to Liquid Crystals: Chemistry and Physics*, 2nd ed. (CRC Press, 2019).

18. H. K. Bisoyi and Q. Li, "Liquid Crystals: Versatile Self-Organized Smart Soft Materials," *Chemical Reviews* 122 (2022): 4887–4926, https://doi.org/10.1021/acs.chemrev.1c00761.

19. J. Uchida, B. Soberats, M. Gupta, and T. Kato, "Advanced Functional Liquid Crystals," *Advanced Materials* 34 (2022): 2109063, https://doi.org/10.1002/adma.202109063.

20. D. S. Miller, X. Wang, and N. L. Abbott, "Design of Functional Materials Based on Liquid Crystalline Droplets," *Chemistry of Materials* 26 (2014): 496–506, https://doi.org/10.1021/cm4025028.

21. J. K. Gupta, S. Sivakumar, F. Caruso, and N. L. Abbott, "Size-Dependent Ordering of Liquid Crystals Observed in Polymeric Capsules With Micrometer and Smaller Diameters," *Angewandte Chemie International Edition* 48 (2009): 1652–1655, https://doi.org/10.1002/anie.200804500.

22. O. D. Lavrentovich, "Topological Defects In Dispersed Words And Worlds Around Liquid Crystals, Or Liquid Crystal Drops," *Liquid Crystals* 24 (1998): 117–126, https://doi.org/10.1080/026782998207640.

23. R. Xie, N. Li, Z. Li, et al., "Liquid Crystal Droplet-Based Biosensors: Promising for Point-of-Care Testing," *Biosensors* 12 (2022): 758, https://doi.org/10.3390/bios12090758.

24. A. Concellón, D. Fong, and T. M. Swager, "Complex Liquid Crystal Emulsions for Biosensing," *Journal of the American Chemical Society* 143 (2021): 9177–9182, https://doi.org/10.1021/jacs.1c04115.

25. M. Abad, A. Martínez-Bueno, and A. Concellón, "Shaping Liquid Crystal Polymer Networks: From Molecular Design and Processing to Multifunctional Materials," *Advanced Materials Technology* 10 (2025): 01236.

26. K. M. Herbert, H. E. Fowler, J. M. McCracken, K. R. Schlafmann, J. A. Koch, and T. J. White, "Synthesis and Alignment Of Liquid Crystalline Elastomers," *Nature Reviews Materials* 7 (2021): 23–28, https://doi.org/10.1038/s41578-021-00359-z.

27. Z.-C. Jiang, Q. Liu, Y.-Y. Xiao, and Y. Zhao, "Liquid Crystal Elastomers For Actuation: A Perspective On Structure-Property-Function Relation," *Progress in Polymer Science* 153 (2024): 101829, https://doi.org/10.1016/j.progpolymsci.2024.101829.

28. H.-F. Lu, M. Wang, X.-M. Chen, B.-P. Lin, and H. Yang, "Interpenetrating Liquid-Crystal Polyurethane/Polyacrylate Elastomer With Ultrastrong Mechanical Property," *Journal of the American Chemical Society* 141 (2019): 14364–14369, https://doi.org/10.1021/jacs.9b06757.

29. Y. Yao, X. Wang, W. Huang, et al., "Low-Temperature Driven Liquid Crystal Elastomer Fibers and Smart Terry Fabrics," *Advanced Functional Materials* (2025): 15319, https://doi.org/10.1002/adfm.202515319.

30. M. Turriani, N. Cosottini, N. Fuochi, D. S. Wiersma, D. Martella, and C. Parmeggiani, "Exploiting Photopolymerization To Modulate Liquid Crystalline Network Actuation," *Soft Matter* 21 (2025): 1162–1169, https://doi.org/10.1039/D4SM01360C.

31. S. Donato, R. Bini, G. Simonetti, et al., "What Is the Right Chain Length? Liquid Crystalline Network Tuning by Molecular Design," *Macromolecules* 58 (2025): 9672–9681, https://doi.org/10.1021/acs.macromol.5c01011.

32. K. Kim, Y. Guo, J. Bae, et al., "4D Printing Of Hygroscopic Liquid Crystal Elastomer Actuators," *Small* 17 (2021): 2100910.

33. J. M. Boothby, H. Kim, and T. H. Ware, "Shape Changes In Chemoresponsive Liquid Crystal Elastomers," *Sensors and Actuators B: Chemical* 240 (2017): 511–518, https://doi.org/10.1016/j.snb.2016.09.004.

34. M. Pilz Da Cunha, S. Ambergen, M. G. Debije, E. F. G. A. Homburg, J. M. J. Den Toonder, and A. P. H. J. Schenning, "A Soft Transporter Robot Fueled by Light," *Advanced Science* 7 (2020): 1902842, https://doi.org/10.1002/advs.201902842.

35. S. Palagi, A. G. Mark, S. Y. Reigh, et al., "Structured Light Enables Biomimetic Swimming And Versatile Locomotion Of Photoresponsive Soft Microrobots," *Nature Materials* 15 (2016): 647–653, https://doi.org/10.1038/nmat4569.

36. H. Xing, J. Li, Y. Shi, J. Guo, and J. Wei, "Thermally Driven Photonic Actuator Based on Silica Opal Photonic Crystal With Liquid Crystal Elastomer," *ACS Applied Materials & Interfaces* 8 (2016): 9440–9445, https://doi.org/10.1021/acsami.6b01033.

37. I. Zubritskaya, D. Martella, and S. Nocentini, "Micropatterned Liquid Crystalline Networks for Multipurpose Color Pixels," *ACS Applied Materials & Interfaces* 17 (2025): 11100–11107, https://doi.org/10.1021/acsami.4c20865.

38. G. Vitale, B. Grandinetti, S. Querceto, et al., "Photoresponsive Polymer-Based Biomimetic Contractile Units as Building Block for Artificial Muscles," *Macromolecular Materials and Engineering* 307 (2022): 2200187, https://doi.org/10.1002/mame.202200187.

39. S. Tasmim, Z. Yousuf, F. S. Rahman, et al., "Liquid Crystal Elastomer Based Dynamic Device For Urethral Support: Potential Treatment For Stress Urinary Incontinence," *Biomaterials* 292 (2023): 121912, https://doi.org/10.1016/j.biomaterials.2022.121912.

40. C. Ohm, E. Fleischmann, I. Kraus, C. Serra, and R. Zentel, "Control of the Properties of Micrometer-Sized Actuators From Liquid Crystalline Elastomers Prepared in a Microfluidic Setup," *Advanced Functional Materials* 20 (2010): 4314–4322, https://doi.org/10.1002/adfm.201001178.

41. E.-K. Fleischmann, F. R. Forst, K. Köder, N. Kapernaum, and R. Zentel, "Microactuators From a main-chain liquid crystalline elastomer via thiol–ene "click" chemistry," *Journal of Materials Chemistry C* 1 (2013): 5885–5891, https://doi.org/10.1039/c3tc30272e.

42. T. Hessberger, L. Braun, and R. Zentel, "Microfluidic Synthesis of Actuating Microparticles From a Thiol-Ene Based Main-Chain Liquid Crystalline Elastomer," *Polymers* 8 (2016): 410, https://doi.org/10.3390/polym8120410.

43. C. Ohm, N. Kapernaum, D. Nonnenmacher, F. Giesselmann, C. Serra, and R. Zentel, "Microfluidic Synthesis of Highly Shape-Anisotropic Particles From Liquid Crystalline Elastomers With Defined Director Field Configurations," *Journal of the American Chemical Society* 133 (2011): 5305–5311, https://doi.org/10.1021/ja1095254.

44. C. Ohm, C. Serra, and R. Zentel, "A Continuous Flow Synthesis of Micrometer-Sized Actuators From Liquid Crystalline Elastomers," *Advanced Materials* 21 (2009): 4859–4862, https://doi.org/10.1002/adma.200901522.

45. J. E. Marshall, S. Gallagher, E. M. Terentjev, and S. K. Smoukov, "Anisotropic Colloidal Micromuscles From Liquid Crystal Elastomers," *Journal of the American Chemical Society* 136 (2014): 474–479, https://doi.org/10.1021/ja410930g.

46. L. B. Braun, T. Hessberger, and R. Zentel, "Microfluidic Synthesis Of Micrometer-Sized Photoresponsive Actuators Based On Liquid Crystalline Elastomers," *Journal of Materials Chemistry C* 4 (2016): 8670–8678, https://doi.org/10.1039/C6TC02587K.

47. D. Ditter, P. Blümler, B. Klöckner, J. Hilgert, and R. Zentel, "Microfluidic Synthesis of Liquid Crystalline Elastomer Particle Transport Systems which Can Be Remote-Controlled Magnetically," *Advanced Functional Materials* 29 (2019): 1902454, https://doi.org/10.1002/adfm.201902454.

48. E.-K. Fleischmann, H.-L. Liang, N. Kapernaum, F. Giesselmann, J. Lagerwall, and R. Zentel, "One-Piece Micropumps From Liquid Crystalline Core-Shell Particles," *Nature Communications* 3 (2012): 1178, https://doi.org/10.1038/ncomms2193.

49. V. S. R. Jampani, D. J. Mulder, K. R. De Sousa, A. Gélébart, J. P. F. Lagerwall, and A. P. H. J. Schenning, "Micrometer-Scale Porous Buckling Shell Actuators Based on Liquid Crystal Networks," *Advanced Functional Materials* 28 (2018): 1801209, https://doi.org/10.1002/adfm.201801209.

50. T. Hessberger, L. B. Braun, F. Henrich, et al., "Co-Flow Microfluidic Synthesis Of Liquid Crystalline Actuating Janus Particles," *Journal of Materials Chemistry C* 4 (2016): 8778–8786, https://doi.org/10.1039/C6TC03378D.

51. T. Hessberger, L. B. Braun, and R. Zentel, "Interfacial Self-Assembly of Amphiphilic Dual Temperature Responsive Actuating Janus Particles," *Advanced Functional Materials* 28 (2018): 1800629, https://doi.org/10.1002/adfm.201800629.

52. M. Liu, J. Fu, and S. Yang, "Synthesis Of Microparticles With Diverse Thermally Responsive Shapes Originated From The Same Janus Liquid Crystalline Microdroplets," *Small* 19 (2023): 2303106.

53. S. Battat, D. A. Weitz, and G. M. Whitesides, "An outlook on microfluidics: The promise and the challenge," *Lab on a Chip* 22 (2022): 530–536, https://doi.org/10.1039/D1LC00731A.

54. L. Shang, Y. Cheng, and Y. Zhao, "Emerging Droplet Microfluidics," *Chemical Reviews* 117 (2017): 7964–8040, https://doi.org/10.1021/acs.chemrev.6b00848.

55. C. Choi, J. Kim, J. Nam, S. Kang, S. Jeong, and C. Lee, "Microfluidic Design of Complex Emulsions," *Chemphyschem* 15 (2014): 21–29, https://doi.org/10.1002/cphc.201300821.

56. A. Concellón, C. A. Zentner, and T. M. Swager, "Dynamic Complex Liquid Crystal Emulsions," *Journal of the American Chemical Society* 141 (2019): 18246–18255, https://doi.org/10.1021/jacs.9b09216.

57. E. M. Sletten and T. M. Swager, "Readily Accessible Multifunctional Fluorous Emulsions," *Chemical Science* 7 (2016): 5091–5097, https://doi.org/10.1039/C6SC00341A.

58. R. V. Balaj and L. D. Zarzar, "Reconfigurable Complex Emulsions: Design, Properties, And Applications," *Chemical Physics Reviews* 1 (2020): 011301, https://doi.org/10.1063/5.0028606.

59. J. Jeong, A. Gross, W.-S. Wei, et al., "Liquid Crystal Janus Emulsion Droplets: Preparation, Tumbling, And Swimming," *Soft Matter* 11 (2015): 6747–6754, https://doi.org/10.1039/C5SM01053E.

60. C. A. Zentner, A. Concellón, and T. M. Swager, "Controlled Movement of Complex Double Emulsions via Interfacially Confined Magnetic Nanoparticles," *ACS Central Science* 2020, 6, 1460–1466, https://doi.org/10.1021/acscentsci.0c00686.

61. L. D. Zarzar, V. Sresht, E. M. Sletten, J. A. Kalow, D. Blankschtein, and T. M. Swager, "Dynamically Reconfigurable Complex Emulsions Via Tunable Interfacial Tensions," *Nature* 518 (2015): 520–524, https://doi.org/10.1038/nature14168.

62. C. A. Zentner, F. Anson, S. Thayumanavan, and T. M. Swager, "Dynamic Imine Chemistry at Complex Double Emulsion Interfaces," *Journal of the American Chemical Society* 141 (2019): 18048–18055, https://doi.org/10.1021/jacs.9b06852.

63. T. Nisisako, H. Suzuki, and T. Hatsuzawa, "Biconvex Polymer Microlenses With Tunable Imaging Properties Designed by Janus Droplet Microfluidics," *Micromachines* 6 (2015): 1435–1444, https://doi.org/10.3390/mi6101428.

64. H. Zappe, "Micro-Optics: A Micro-Tutorial," *Advanced Optical Technologies* 1 (2012): 117–126, https://doi.org/10.1515/aot-2012-0016.

65. K. Perera, N. Haputhantrige, M. S. H. Himel, et al., "Electrically Tunable Polymer Stabilized Chiral Ferroelectric Nematic Liquid Crystal Microlenses," *Advanced Optical Materials* 12 (2024): 2302500, https://doi.org/10.1002/adom.202302500.

Supporting Information

Additional supporting information can be found online in the Supporting Information section.

Supporting File 1: adfm74133-sup-0001-SuppMat.pdf.
Supporting File 2: adfm74133-sup-0002-MovieS1.mp4.
Supporting File 3: adfm74133-sup-0003-MovieS2.mp4.
Supporting File 4: adfm74133-sup-0004-MovieS3.mp4.
Supporting File 5: adfm74133-sup-0005-MovieS4.mp4.